International Journal of Nanomedicine

Dovepress
Taylor & Francis Group

Open Access Full Text Article

ORIGINAL RESEARCH

Umbilical Cord Mesenchymal Stem Cell-Derived Extracellular Nanovesicles Alleviated Colitis via Modulating Th17/Treg Balance Through Hsa-miR-27b-3p-Mediated Suppression of PI3K/AKT/STAT3 Signaling Pathway

Yuanhao Zhou[1–3,*], Yuanyuan Wang[1–3,*], Yilin Huang[1,2], Ping Li[1,2], Yan Zeng[1,2], Weijiao Fan[1,2], Zhiwei Lin[4], Xiangming Ye[1], Jinyang Chen[4], Ketao Jin[5], Xiaozhou Mou[1,2], Xiaoyi Chen[1,2]

[1]Center for Rehabilitation Medicine, Rehabilitation and Sports Medicine Research Institute of Zhejiang Province, Department of Rehabilitation Medicine, Zhejiang Provincial People's Hospital (Affiliated People's Hospital), Hangzhou Medical College, Hangzhou, Zhejiang, 310014, People's Republic of China; [2]Zhejiang Key Laboratory of Tumor Molecular Diagnosis and Individualized Medicine, Clinical Research Institute, Zhejiang Provincial People's Hospital, Affiliated People's Hospital, Hangzhou Medical College, Hangzhou, Zhejiang, 310014, People's Republic of China; [3]MOE Key Laboratory of Macromolecular Synthesis and Functionalization, Department of Polymer Science and Engineering, Zhejiang University, Hangzhou, Zhejiang, 310027, People's Republic of China; [4]HealthRegen (Hangzhou) Biotechnology Co., Ltd., Hangzhou, Zhejiang, 310000, People's Republic of China; [5]Department of Colorectal and Anal Surgery, The First Affiliated Hospital of Zhejiang Chinese Medical University (Zhejiang Provincial Hospital of Chinese Medicine), Hangzhou, Zhejiang, 310003, People's Republic of China

*These authors contributed equally to this work

Correspondence: Xiaozhou Mou; Xiaoyi Chen, Email mouxz@zju.edu.cn; chenxiaoyi@hmc.edu.cn

Background: Inflammatory bowel disease (IBD) is a chronic inflammatory disorder of the gastrointestinal tract, characterized by persistent immune dysregulation. Umbilical cord mesenchymal stem cell-derived extracellular nanovesicles (MSC NVs) exhibit immunomodulatory properties, demonstrating significant therapeutic potential for clinical applications. This study sought to investigate the therapeutic effects of MSC NVs against colitis and elucidate the underlying mechanisms.

Methods: MSC NVs were prepared from umbilical cord MSCs using a continuous filtration-extrusion method. The therapeutic effects of MSC NVs were assessed by tail vein injection in a murine model of DSS-induced colitis.

Results: MSC NVs significantly markedly ameliorated colitis-associated symptoms, including body weight loss, colon length reduction, and elevated disease activity index scores. MSC NVs not only mitigated colitis-induced intestinal barrier impairment and inflammatory responses, but also exhibited targeted biodistribution to inflamed colonic lesions. Unexpectedly, administration of MSC-NVs via the tail vein significantly altered the gut microbial composition in colitic mice, particularly enhancing the relative abundances of beneficial commensal genera *Lachnoclostridium* and *Dubosiella*, consequently reestablishing microbial homeostasis. Moreover, MSC NVs modulated the T help (Th) 17/ regulatory T (Treg) balance within the colonic lamina propria through delivery of hsa-miR-27b-3p, which directly targeted the PIK3CA gene, thereby inhibiting PI3K/AKT/STAT3 signaling pathway activation and exerting anti-colitis effects.

Conclusion: This study demonstrated that MSC NVs significantly alleviated DSS-induced colitis by modulating Th17/Treg balance in the colonic lamina propria, with hsa-miR-27b-3p identified as the key mediator through PIK3CA targeting and PI3K/AKT/STAT3 pathway inhibition. These findings highlight the therapeutic potential of filtration–extrusion-prepared MSC NVs as a safe and effective nanomedicine for IBD treatment.

Keywords: colitis, umbilical cord mesenchymal stem cells, extracellular nanovesicles, Th17/Treg balance, microRNAs, PI3K/AKT/STAT3 pathway

Received: 26 September 2025
Accepted: 10 December 2025
Published: 25 December 2025

Graphical Abstract

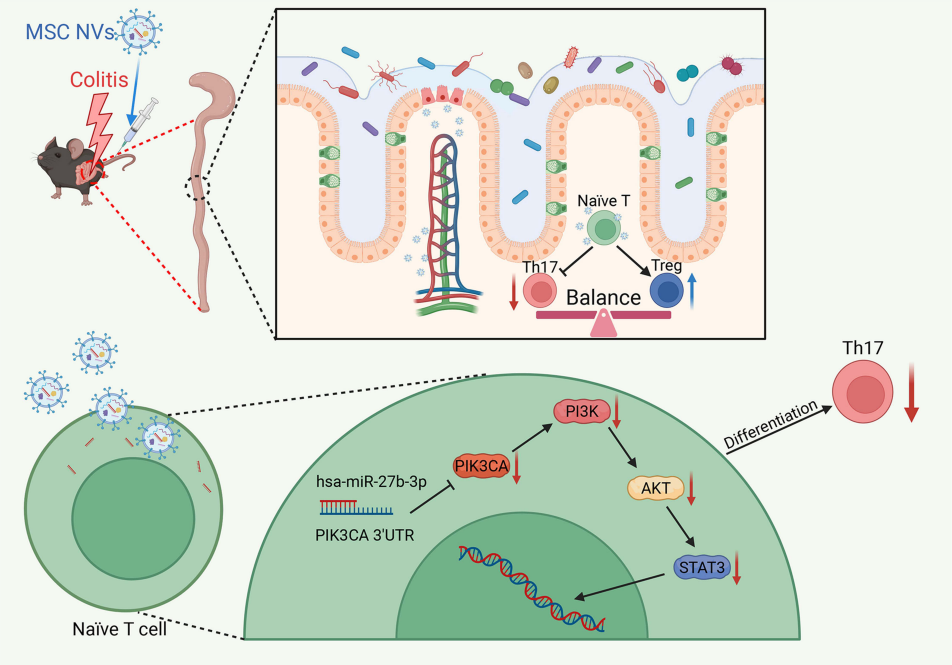

Introduction

Inflammatory bowel disease (IBD), encompassing Crohn's disease (CD) and ulcerative colitis (UC), represents chronic and recurrent inflammatory disorders of the gastrointestinal tract characterized by abdominal pain, diarrhea, hematochezia, and maldigestion.[1,2] Currently, the mainstay therapeutic approaches for IBD comprise immunosuppressive therapy and surgical intervention.[3] Nevertheless, the substantial risks of infectious and neoplastic disease associated with chronic immunosuppressive therapy evoke significant clinical concerns, while surgical interventions carry inherent risks of digestive function impairment.[4] Consequently, developing safe and effective therapeutic strategies for IBD patients has become an urgent clinical necessity.

Mesenchymal stem cell (MSC) therapy is a promising cell-based therapeutic strategy for IBD, with its principal mechanisms being the suppression of inflammation, the regulation of immune dysregulation, and the promotion of mucosal repair.[5] At present, the most extensively investigated MSCs are those derived from umbilical cord, adipose tissue, and bone marrow. MSCs modulate the immune system through multiple mechanisms, such as inhibiting the differentiation of monocytes into dendritic cells, suppressing T cell activation by down-regulating co-stimulatory molecules on mature dendritic cells, and inducing the generation of regulatory T (Treg) cells.[6] However, MSC therapy is constrained by both a prolonged induction period and non-negligible tumorigenic risks, thereby limiting its clinical application.[7] To overcome these limitations, cell-free therapy employing stem cell-derived extracellular vesicles presents a novel therapeutic approach, as it avoids risks inherent to living, replicating cells while retaining the beneficial properties of MSCs.[8]

Extracellular nanovesicles (ENVs), defined as nanoscale membrane vesicles of 30–1000 nm diameter, are actively secreted by cells.[9] ENVs exhibit the capacity to deliver a diverse array of bioactive molecules, including proteins, lipids, mRNAs, microRNAs, and other genetic materials, into recipient cells, thereby modulating the activity of these cells.[10] Among the bioactive molecules carried by ENVs, microRNAs (miRNAs) have been identified as pivotal regulators of a broad spectrum of physiological and pathological processes.[11] ENVs function as critical mediators of intercellular communication, facilitating the transfer of diverse molecules and signaling factors between cells. Notably, MSC-derived extracellular nanovesicles (MSC NVs) effectively replicate the immunomodulatory and tissue-repair

capacities of their source cells.[12] Furthermore, MSC NVs exhibit multiple advantageous properties, including high stability, low immunogenicity, negligible tumorigenic potential, targeted homing capability, and no risk of vascular occlusion.[13,14] Currently, our laboratory has optimized a continuous filtration-extrusion approach for umbilical cord MSC NVs production, achieving significantly higher production yields compared to traditional ultracentrifugation methods.[15]

Among $CD4^+$ T cell subsets, both T help (Th)17 cells and Tregs play critical roles in maintaining intestinal mucosal immune homeostasis. Th17 cells mediate intestinal mucosal defense against microbial pathogens through secretion of IL-17 and IL-22, which stimulate innate immune activation, neutrophil recruitment, and epithelial antimicrobial peptide production, while concurrently promoting inflammatory responses and tissue injury.[16] Tregs sustain intestinal immune homeostasis through secretion of IL-10 and TGF-β, which suppress proinflammatory responses and maintain immune tolerance.[17] Th17 cells and Tregs, derived from naïve $CD4^+$ T cells, exhibit reciprocal inhibition in the intestinal immune microenvironment to coordinately regulate immune homeostasis.[18] In colonic mucosal tissues of colitis patients, elevated IL-17A levels and increased Th17 cell populations demonstrate the pivotal involvement of Th17/Treg imbalance in colitis pathogenesis and disease progression.[19,20] Therefore, therapeutic strategies aimed at restoring Th17/Treg emerge as a promising approach for IBD.[18]

Considering the therapeutic potential of MSC NVs generated through continuous filtration-extrusion method in both nanomedicine and clinical practice, this study systematically investigates their therapeutic efficacy in DSS-induced colitis, immunomodulatory properties, and underlying mechanisms.

Materials and Methods

Isolation and Identification of Umbilical Cord MSCs

Experiment protocols were approved by the Ethics Committee of Zhejiang Provincial People's Hospital (No. KT2022025). This study was conducted in accordance with the Declaration of Helsinki. Human MSCs were isolated from full-term umbilical cord according to standardized protocols established in our laboratory.[15] Briefly, umbilical cord tissues were minced into 1 mm^3 fragments, rinsed with sterile PBS, centrifuged, and resuspended in serum-free culture medium (Lonza, Walkersville, MD, USA) for subsequent culture. When second- to third-passage MSCs reached 70% confluence, they were serum-starved for 48 h prior to collection for identification and further experiments.

The harvested MSCs were characterized by flow cytometry using the following surface markers: CD90 (BD Pharmingen), CD105 (BD Pharmingen), CD73 (BD Pharmingen) as positive markers, and CD45 (BD Pharmingen), CD14 (BD Pharmingen), CD34 (BD Pharmingen), HLA-DR (BD Pharmingen) as negative markers.

Isolation and Identification of MSC NVs

At 70% confluence, MSCs were collected, resuspended at a concentration of $2–3\times10^6$/mL, and sequentially extruded through polycarbonate films with decreasing pore sizes (10 μm, 5 μm, 1 μm, 400 nm, and 200 nm) for 11–21 cycles. The extruded vesicles were subjected to horizontal centrifugation (4 °C, 10 min), followed by supernatant collection. The sample was then subjected to two sequential centrifugation steps: initial clarification at 2000 × g (4 °C, 20 min) followed by vesicle pelleting at 10,000 × g (4 °C, 30 min) using a fixed-angle rotor. The resulting supernatant was sterile-filtered through a 0.22 μm membrane. The sample was then ultracentrifuged at 100,000 × g (4 °C, 70 min) using a swinging-bucket rotor. Following supernatant removal, the pelleted nanovesicles were resuspended in ice-cold PBS and cryopreserved at −80°C.

MSC NV suspensions were dropped onto copper grids, negatively stained with phosphotungstic acid, and examined using transmission electron microscopy (Hitachi H-7650, Hitachi, Ibaraki, Japan). The particle size distribution and zeta potential of MSC NVs were detected by dynamic light scattering (Malvern Instruments, Worcestershire, UK). The markers of the MSC NVs, including CD9 (BD Pharmingen), CD63 (Biolegend), and CD81 (Biolegend), were analyzed using the Flow NanoAnalyzer (Vdobiotech, Suzhou, China).

Animal Models

All animal experiments were performed in compliance with protocols approved by the Animal Ethics Committee of Zhejiang Provincial People's Hospital (IACUC Issue No. 20231012144405179262). Male C57BL/6 mice (4 weeks old) were obtained from SLAC Laboratory Animal Co., Ltd. (Shanghai, China), kept under specific-pathogen-free conditions with ad libitum access to food and water.

After one week of acclimatization, mice were randomly allocated into four groups (n = 8/group): Control, DSS, MSC NVs-L, MSC NVs-H. Colitis was induced in DSS and both MSC NVs treatment group by administering 2.5% (*w*/*v*) DSS (MP Biomedicals, Santa Ana, CA, USA) in drinking water for 7 days. On days 3, 6, and 9 post-DSS induction, MSC NVs-L and MSC NVs-H groups received 2×10^9 and 2×10^{10} particles of MSC NVs, respectively, through tail vein injection. Control and DSS group mice received equivalent volumes of sterile PBS via identical injection protocols. Body weight changes and disease activity index (DAI) scores were recorded daily, with DAI scoring criteria adapted from Kaur et al.[21]

All mice euthanized on day 11. Individual mice were euthanized in a clean chamber by gradual-fill CO_2 inhalation at a flow rate displacing 30% of the chamber volume per minute. All procedures were designed to minimize animal suffering in accordance with the guidelines for animal care (GB/T 39760–2021, China).

Intestinal Permeability Assay

Following a 6-hour fast, mice received 0.6 mg/g body weight of 4 kDa FITC-dextran (Sigma-Aldrich, St. Louis, MO, USA) via oral gavage. Blood was collected 4 hours post-administration, and serum FITC-dextran levels were quantified by fluorescence measurement (excitation, 495nm; emission, 525nm). FITC-dextran concentrations were determined by interpolation from a standard curve.

Histopathology

Colon tissues were fixed in 4% (*v*/*v*) paraformaldehyde (Beyotime, Shanghai, China), dehydrated, and subsequently embedded in paraffin. Tissue sections (5 μm) were stained with either hematoxylin and eosin (H&E) or alcian blue-periodic acid-Schiff (AB-PAS). Histopathological images were acquired using light microscope, with histological scoring performed using the established criteria by Stillie and Stadnyk.[22]

Immunofluorescence

Colon sections underwent sequential processing including: dewaxing, rehydration, antigen retrieval, blocking, and incubation with primary antibodies (occludin + claudin-1, Servicebio, Wuhan, China) and corresponding secondary antibodies (Servicebio, Wuhan, China). Nuclei were counterstained with DAPI (Beyotime, Shanghai, China), and images were acquired by laser scanning confocal microscopy followed by quantitative analysis using ImageJ.

ELISA

Serum cytokine concentrations (IL-1β, TNF-α, IFN-γ, IL-6, IL-12 p70, and IL-17A) were quantified using commercial ELISA kits (Abclonal, Wuhan, China) according to the protocols.

Live Image Tracking of MSC NVs

MSC NVs were labeled with DIR dye (LABLEAD, Beijing, China) according to the instruction. The gastrointestinal tract, heart, liver, spleen, lungs, and kidneys of the mice were collected at 0.5, 1, 2, 4, 6, 12, 24, and 36 hours post-injection and imaged using the IVIS Spectrum system (PerkinElmer, Waltham, MA, USA) to monitor the distribution of MSC NVs.

RNA Sequencing and Analysis

Total RNA was extracted from the colonic tissue of mice and utilized for library construction. The library preparations were sequenced (paired-end) on the Illumina NovaSeq X Plus platform. Raw sequencing reads were quality-filtered and aligned to the reference genome. Differentially expressed genes were identified using the following criteria: log2 (Fold

change) ≥ 1 and p-value ≤ 0.05. Functional enrichment analysis of differentially expressed genes was performed using Gene Ontology (GO) and Kyoto Encyclopedia of Genes and Genomes (KEGG) databases.

Isolation and Identification of Intestinal Innate Lymphoid Cells

Minced colonic tissue was enzymatically digested with collagenase IV (Absin, Shanghai, China) and DNase I (Sigma-Aldrich, St. Louis, MO, USA). The digested solution was filtered through a 70-μm mesh filter, followed by density gradient centrifugation (40%/80% Percoll). Lymphocytes were isolated from the interphase layer for downstream analysis.

Lymphoid cells were activated using leukocyte activation cocktail (BD Pharmingen, San Jose, CA, USA), followed by sequential processing: Fc receptor blockade (BD Pharmingen, San Jose, CA, USA), surface staining (CD3, BD Pharmingen; CD4, BD Pharmingen; CD25, BD Pharmingen; CD45, BD Pharmingen), fixation and permeabilization (BD Pharmingen, San Jose, CA, USA), and intracellular staining (IL-17A, BD Pharmingen; Foxp3, Thermo Fisher). Samples were analyzed using flow cytometry. Flow cytometry gating scheme was shown in Figure S1.

Intestinal Microbiota Analysis

Fecal genomic DNA was used to amplify the V3-V4 regions of the bacterial 16S rDNA gene using primers 338F (5′- ACTCCTACGGGAGGCAGCA-3′) and 806R (5′- GGACTACHVGGGTWTCTAAT-3′). The amplified sequences were examined using the Illumina MiSeq platform. Raw sequences were quality-filtered and clustered into operational taxonomic units (OTUs) at 97% similarity using QIIME software. Microbial community diversity was analyzed using QIIME software, including α-diversity indices (Shannon diversity index, Ace and Chao richness estimators, and observed species, Sobs), as well as β-diversity. β-diversity was visualized through principal-coordinate analysis (PCoA) plots. Microbial composition was analyzed at the genus taxonomic level.

Quantitative Real-Time PCR

For mRNA analysis, total RNA was extracted from colonic tissues utilizing RNAiso Plus (Takara, Dalian, China), reverse transcribed with HiScript II Q Select RT SuperMix (Vazyme, Nanjing, China), and quantified using ChamQ Universal SYBR qPCR Master Mix (Vazyme, Nanjing, China) on the StepOne^{TM} Plus Real-Time PCR system (Applied Biosystems, Carlsbad, CA, USA). Primer sequences are listed in Table S1. β-actin was utilized as the endogenous gene, and relative gene expressions were quantified using the $2^{-\Delta\Delta Ct}$ method.

For miRNA analysis, total RNA was extracted utilizing RNAiso Plus (Takara, Dalian, China), reverse transcribed with the EZ-press microRNA Reverse Transcription Kit (EZBioscience, Jiangsu, China), and quantified using EZ-press microRNA qPCR Kit (EZBioscience, Jiangsu, China) on the StepOne^{TM} Plus Real-Time PCR system. Primer sequences are listed in Table S2. U6 small nuclear RNA was utilized as the endogenous gene, and relative miRNA expressions were quantified using the $2^{-\Delta\Delta Ct}$ method.

Western Blot Analysis

Colon tissue lysates were quantified using a BCA Kit (Beyotime, Shanghai, China). Protein samples were separated by SDS-PAGE and transferred to PVDF membranes (Millipore, Billerica, MA, USA). Membranes were blocked and incubated with primary antibodies: Phosphatidylinositol 3-kinase (PI3K, Cell Signaling Technology, Danvers, MA, USA), Phospho-PI3K (Cell Signaling Technology, Danvers, MA, USA), PI3K–protein kinase B (AKT, Abclonal, Wuhan, China), Phospho-AKT (Abclonal, Wuhan, China), signal transducer and activator of transcription 3 (STAT3, Cell Signaling Technology, Danvers, MA, USA), Phospho-STAT3 (Cell Signaling Technology, Danvers, MA, USA) and β-actin (Abcam, Cambridge, UK). Following incubation with HRP-conjugated secondary antibodies (Abclonal, Wuhan, China). Protein bands were detected using an imaging equipment (Bio-Rad). Protein band intensities were quantified with ImageJ software.

miRNA Sequencing and Analysis

Total RNA was extracted from the MSC NVs for small RNA library preparation. Libraries were size-selected (18–26 nt) and sequenced on an Illumina HiSeq 2000/2500 platform. Raw sequencing reads were quality-filtered and aligned to

obtain clean data. miRNA annotation was conducted by aligning to miRBase database. Target mRNAs and miRNA binding sites were predicted using StarBase, TarBase, and TargetScan databases.

Cell Culture

HEK293T or Raw264.7 cells were cultivated in high glucose Dulbecco's Modified Eagle Medium supplemented with 10% fetal bovine serum (FBS, Hangzhou Yangming Biotechnology Co., LTD., Hangzhou, China), 100 U/mL penicillin, and 100 μg/mL streptomycin, and maintained at 37 °C with 5% CO_2.

Dual-Luciferase Reporter Gene Assay

The 3′-untranslated region (3′UTR) of PIK3CA containing the predicted hsa-miR-27b-3p wild-type and mutated binding sites were cloned to plasmid PGL3-CMV-LUC (Genomeditech, Shanghai, China) to construct plasmids pGL3-CMV-LUC-H_PIK3CA 3'UTR WT and pGL3-CMV-LUC-H_PIK3CA 3'UTR MT, respectively. Plasmids and miRNA mimics were co-transfected into HEK293T cells using GMTrans Liposomal Transfection Reagent (Genomeditech, Shanghai, China). Luciferase activity was detected using the dual-luciferase reporter gene assay kit (Genomeditech, Shanghai, China). Plasmid sequencing primers, verification results, and siRNA sequences are listed in Tables S3–S5, respectively.

miRNA Mimics Transfection

Normal Control (NC) mimics and hsa-miR-27b-3p mimics were transfected into HEK293T cells using Lipofectamine 3000 (Sigma-Aldrich, St. Louis, MO, USA), respectively. Cellular total RNA and protein were extracted for further experiments.

Biosafety Assay of MSC NVs

After one week of acclimatization, mice were randomly allocated into three groups (n = 5/group): Control, MSC NVs-L, MSC NVs-H. On days 3, 6, and 9 post-grouping, MSC NVs-L and MSC NVs-H groups received 2×10^9 and 2×10^{10} particles of MSC NVs, respectively, via tail vein injection. Control group mice received equivalent volumes of sterile PBS. On day 11, all animals were euthanized after daily body weight monitoring. Serum, heart, liver, spleen, lungs, kidneys, and colon were collected to determine biochemical indicators (aspartate aminotransferase, AST; alanine aminotransferase, ALT; creatinine, CREA; urea, UREA) and prepare H&E sections.

Cellular Uptake

To evaluate the cellular uptake of MSC NVs, RAW264.7 cells were seeded in confocal dishes at a density of 1×10^5 cells/dish and cultured for 24 h. MSC NVs were labeled with DIO dye (LABLEAD, Beijing, China) according to the instruction. The cells were then treated with DIO-labeled MSC NVs for 24 h at 37°C. Following incubation, the cells were washed thrice with PBS and the nuclei were counterstained with DAPI (Beyotime, Shanghai, China). After three additional PBS washes, the samples were imaged using a laser scanning confocal microscope (Leica, Wetzlar, Germany).

Statistical Analysis

Data were analyzed using SPSS software and given as mean ± standard deviation (SD). Intergroup comparisons were analyzed by two-tailed Student's *t*-test (two groups) or one-way ANOVA with Tukey's post-hoc test (multiple groups). Differences were deemed statistically significant when p-value < 0.05. Graphs were generated using Prism 9 (GraphPad, San Diego, CA, USA).

Results

Preparation and Characterization of MSC and MSC NVs

The isolation procedure for MSCs and MSC NVs is schematically depicted in Figure 1A. Flow cytometry confirmed that the isolated human umbilical cord-derived cells exhibited typical MSC surface marker profiles, with high

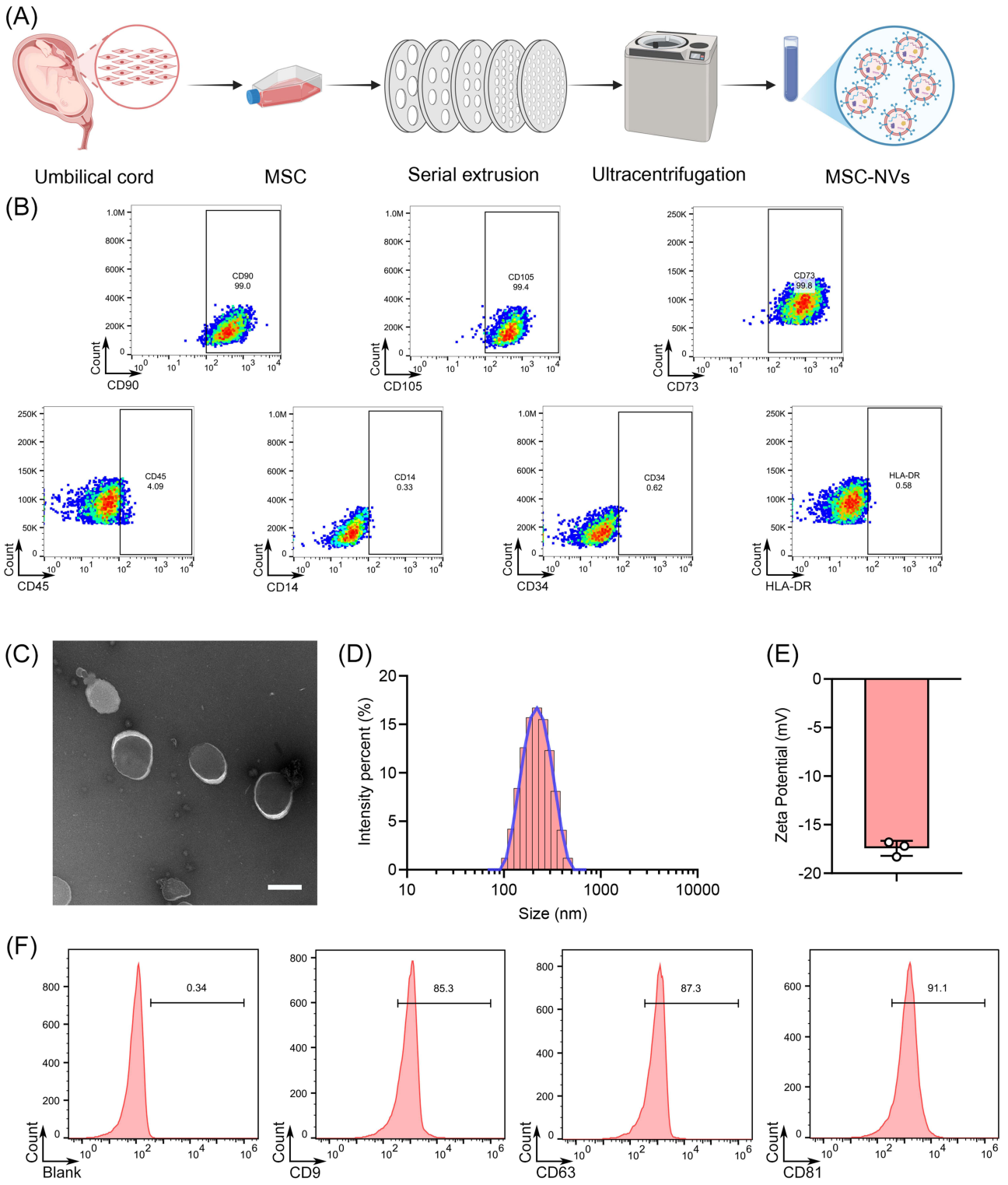

Figure 1 Isolation and physicochemical characterization of MSC NVs derived from MSCs. (**A**) Schematic diagram of the isolation process of MSC NVs. (**B**) Flow cytometry analysis of surface markers on MSCs. (**C**) Representative TEM images of MSC NVs (Scar bar, 200 nm). (**D**) The particle size distribution of MSC NVs. (**E**) The zeta potential of MSC NVs. (**F**) Flow cytometry analysis of surface markers on MSC NVs.

expression of CD90, CD105, and CD73, while lacking expression of CD45, CD14, CD34, and HLA-DR (Figure 1B). Transmission electron microscopy analysis confirmed that the isolated MSC NVs exhibited intact bilayer membrane structures, thereby confirming their typical extracellular nanovesicle morphology (Figure 1C).

https://doi.org/10.2147/IJN.S565416

Dynamic light scattering analysis indicated that the size distribution of MSC NVs ranged from 105.7 nm to 458.7 nm, with a mean size of 182.4 nm (Figure 1D). Additionally, zeta potential measurements revealed that these ENVs possessed a surface charge of −17.43 ± 0.78 mV (Figure 1E). Flow NanoAnalyzer analysis confirmed CD9, CD63, and CD81 positivity in MSC NVs (Figure 1F). Together with our previous Western blot data which demonstrated the expression of CD63, CD81, and TSG101,[15] these results collectively indicate that MSC NVs exhibit extracellular vesicle-like properties following mechanical extrusion.

MSC NVs Mitigated DSS-Induced Colitis

To evaluate the therapeutic effects of MSC NVs on DSS-induced colitis, mice received intravenous tail vein injections of either 2×10^9 (MSC NVs-L) or 2×10^{10} (MSC NVs-H) particles on days 3, 6, and 9 (Figure 2A). DSS administration induced characteristic colitis manifestations, including considerable weight loss, increased DAI scores, and reduced colon length. Notably, both MSC NVs-treated groups demonstrated significant mitigation of these pathological symptoms (Figure 2B–E). Among them, the low-concentration MSC NVs group exhibited the best therapeutic efficacy, exhibiting significantly greater final body weight recovery compared to the high-concentration group (Figure 2B). Furthermore, intestinal permeability assays revealed that both MSC NVs-treated groups exhibited significantly reduced systemic fluorescence intensity compared to the DSS group, indicating restoration of intestinal barrier function (Figure 2F). MSC NVs treatment significantly mitigated DSS-induced colonic ulcers, inflammatory infiltration, crypt loss, goblet cells depletion, and decreased mucin 2 gene expression (Figure 2G–I).

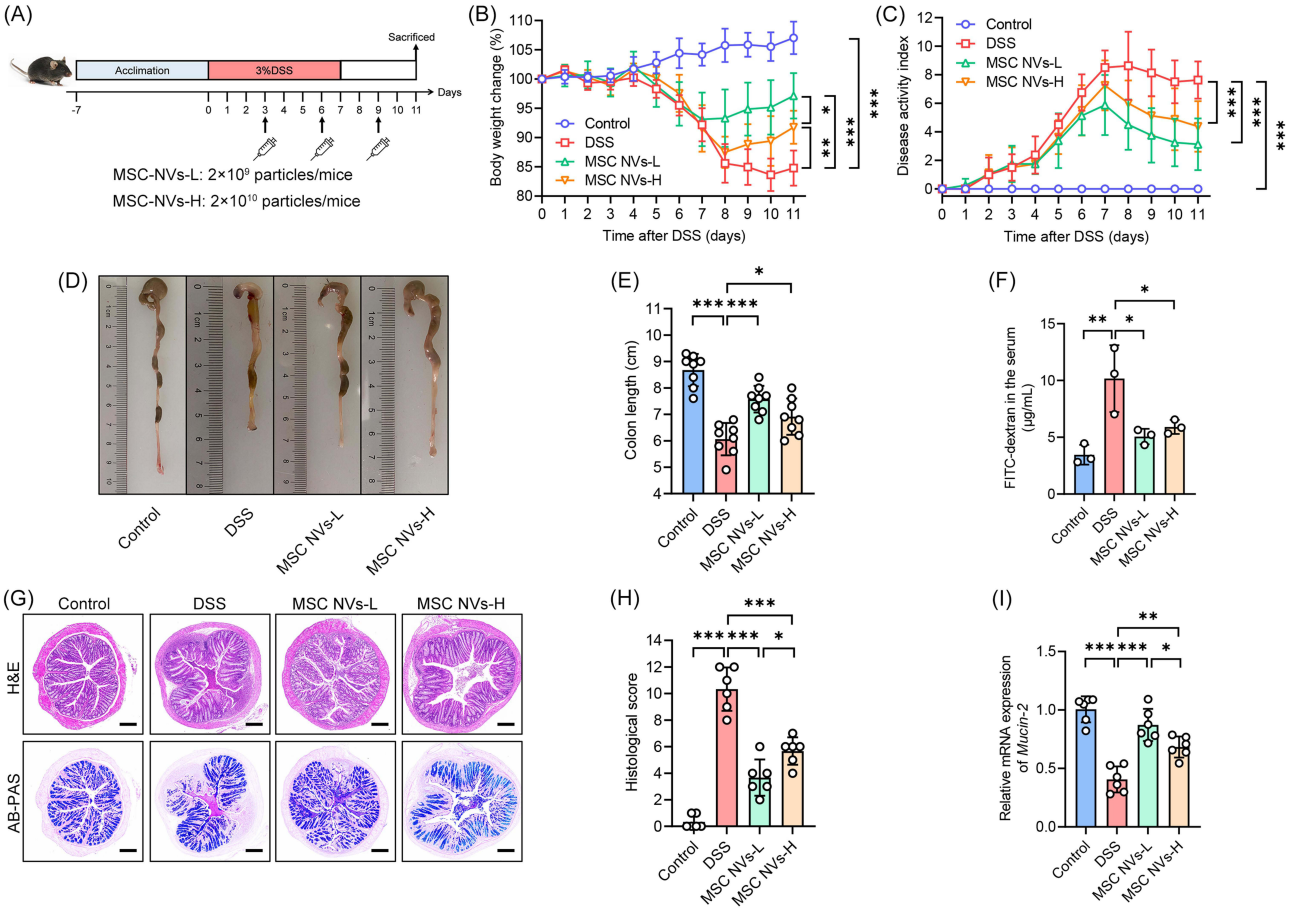

Figure 2 MSC NVs alleviated DSS-induced colitis and mitigated colonic tissue damage. (**A**) Schematic illustration of experimental design. (**B**) Body weight change. (**C**) DAI assessment. (**D**) Representative pictures of colon. (**E**) The length of the colon. (**F**) Intestinal barrier function assessment. (**G**) Representative micrographs of H&E (Scale bar, 200 μm) and AB-PAS (Scale bar, 200 μm). (**H**) Histology score of H&E staining. (**I**) Relative gene expression of *mucin 2* in the colon. Means ± SD; *$p < 0.05$, **$p < 0.01$, ***$p < 0.001$.

MSC NVs Facilitated the Restoration of Intestinal Tight Junctions

The disruption of the integrity of intestinal tight junctions, which are key components of the intestinal barrier, will lead to intestinal dysfunction [39]. In the current study, DSS administration significantly decreased the protein expression of the tight junction proteins occludin and claudin-1 in the colonic tissues of mice (Figure 3A and B), while concurrently reducing the gene expression of occludin, claudin-1, and ZO-1 (Figure 3C). On this basis, both MSC NVs-L and MSC

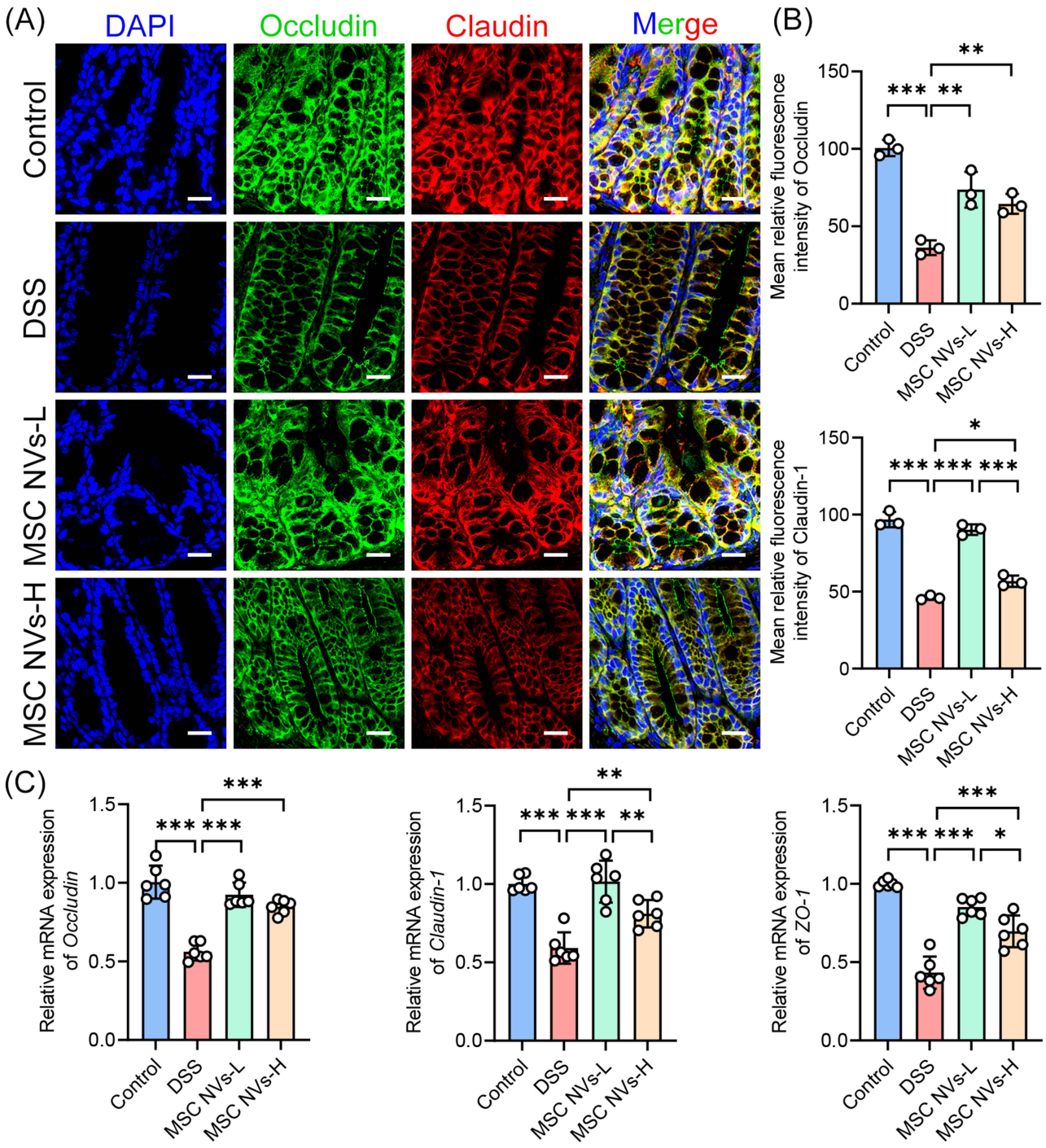

Figure 3 MSC NVs attenuated tight junction damage induced by colitis. (**A**) Immunofluorescence analysis for occludin (greed) and claudin-1 (red) in the colon. Nuclei (DAPI, blue) (Scale bar, 20 μm). (**B**) Mean relative fluorescence intensity of occludin and claudin-1 in Figure 3A. (**C**) Relative gene expression of occludin, claudin-1 and zo-1 in the colon. Means ± SD; *$p < 0.05$, **$p < 0.01$, ***$p < 0.001$.

https://doi.org/10.2147/IJN.S565416

NVs-H significantly enhanced gene and protein expressions of occludin, claudin-1, and ZO-1 in the colonic tissues of colitic mice. Moreover, both protein and gene expression levels of claudin-1, along with ZO-1 gene expression, were significantly higher in the MSC NVs-L group compared with the MSC NVs-H group (Figure 3A–C).

MSC NVs Attenuated DSS-Induced Inflammation

To further evaluate the impact of MSC NVs on systemic inflammation elicited by colitis, serum pro-inflammatory cytokine levels were measured. DSS administration drastically increased serum concentrations of IL-1β, TNF-α, IFN-γ, IL-6, IL-12 p70, and IL-17A, indicating occurrence of severe inflammation. Notably, MSC NVs-L treatment significantly reduced serum concentrations of IL-1β, TNF-α, IFN-γ, IL-6, and IL-17A in colitic mice, while MSC NVs-H only showed significant reduction in TNF-α, IFN-γ, and IL-6 concentrations (Figure 4A). Despite the differential efficacy between the two groups, a direct comparison of serum pro-inflammatory cytokine levels showed no statistically significant difference. Given that the superior therapeutic efficacy of low-concentration MSC NVs (2×10^9 particles) compared to high-concentration MSC NVs (2×10^{10} particles) in ameliorating murine colitis, all subsequent investigations were exclusively conducted in the low-concentration MSC NVs group.

In vivo Distribution of MSC NVs in Mice with Colitis

Following successful induction of colitis, mice received a single intravenous injection of DIR-labeled MSC NVs through the tail vein. As shown in Figure 4B, DIR-labeled MSC NVs were detectable in the stomach and cecum of colitic mice as early as 0.5 h post-intravenous administration. Subsequently, fluorescence was progressively detected in the colon, ileum, and jejunum as time elapsed. The fluorescence intensity in the colon reached its maximum at 24 h post-injection, followed by a gradual decline. Regarding the distribution of DIR-labeled MSC NVs in the organs, the liver exhibited the most pronounced fluorescence intensity at all timepoints, whereas the fluorescence intensity in the heart, spleen, lungs, and kidneys was comparatively weaker.

MSC NVs Modulated the Immune Response in Mice with Colitis

To investigate the therapeutic mechanisms of MSC NVs in DSS-induced colitis, RNA sequencing was conducted on colonic tissues (Figure 5A). Differential gene expression analysis identified 269 significantly upregulated genes and 656 significantly downregulated genes in DSS-treated mice compared to controls (Figure 5B). Administration of MSC NVs via tail vein injection induced significant gene expression alterations, with 260 genes showing upregulation and 370 genes demonstrating downregulation compared to the DSS group (Figure 5C). Subsequently, GO enrichment analysis was conducted to elucidate the potential pathways associated with these differentially expressed genes (Figure 5D). GO enrichment analysis revealed significant enrichment of differentially expressed genes (MSC NVs-L vs DSS) in immune regulatory pathways, such as regulation of regulatory T cell differentiation, production of molecular mediator of immune response, neutrophil migration, T cell mediated immunity, regulation of Th17 cell differentiation, regulation of macrophage cytokine production, and IL-17 production. Additionally, GO enrichment analysis identified significant enrichment of differentially expressed genes in pathways related to antibacterial immune responses, such as response to molecule of bacterial origin, response to lipopolysaccharide, antimicrobial humoral response, regulation of phagocytosis, and defense response to gram-positive bacterium. These findings indicate that MSC NVs effectively regulate immune homeostasis in mice with colitis. Similarly, KEGG enrichment analysis further revealed that differentially expressed genes were implicated in immune regulation-related pathways, including IL-17 signaling pathway, PI3K-Akt signaling pathway, cytokine-cytokine receptor interaction, and inflammatory bowel disease, as well as pathways associated with antibacterial defense immune mechanisms, such as toll-like receptor signaling pathway and PPAR signaling pathway (Figure 5E). The KEGG pathway enrichment analysis further substantiate the immunomodulatory function of MSC NVs in colitis.

MSC NVs Modified the Microbiota in Mice with Colitis

Given that RNA sequencing data revealed the involvement of MSC-NVs in antibacterial immune responses, the effects of MSC NVs on the gut microbiota in colitis were further investigated. As shown in Figure 6A, compared with the control group, the DSS group exhibited significant alterations in gut microbiota α-diversity, characterized by marked

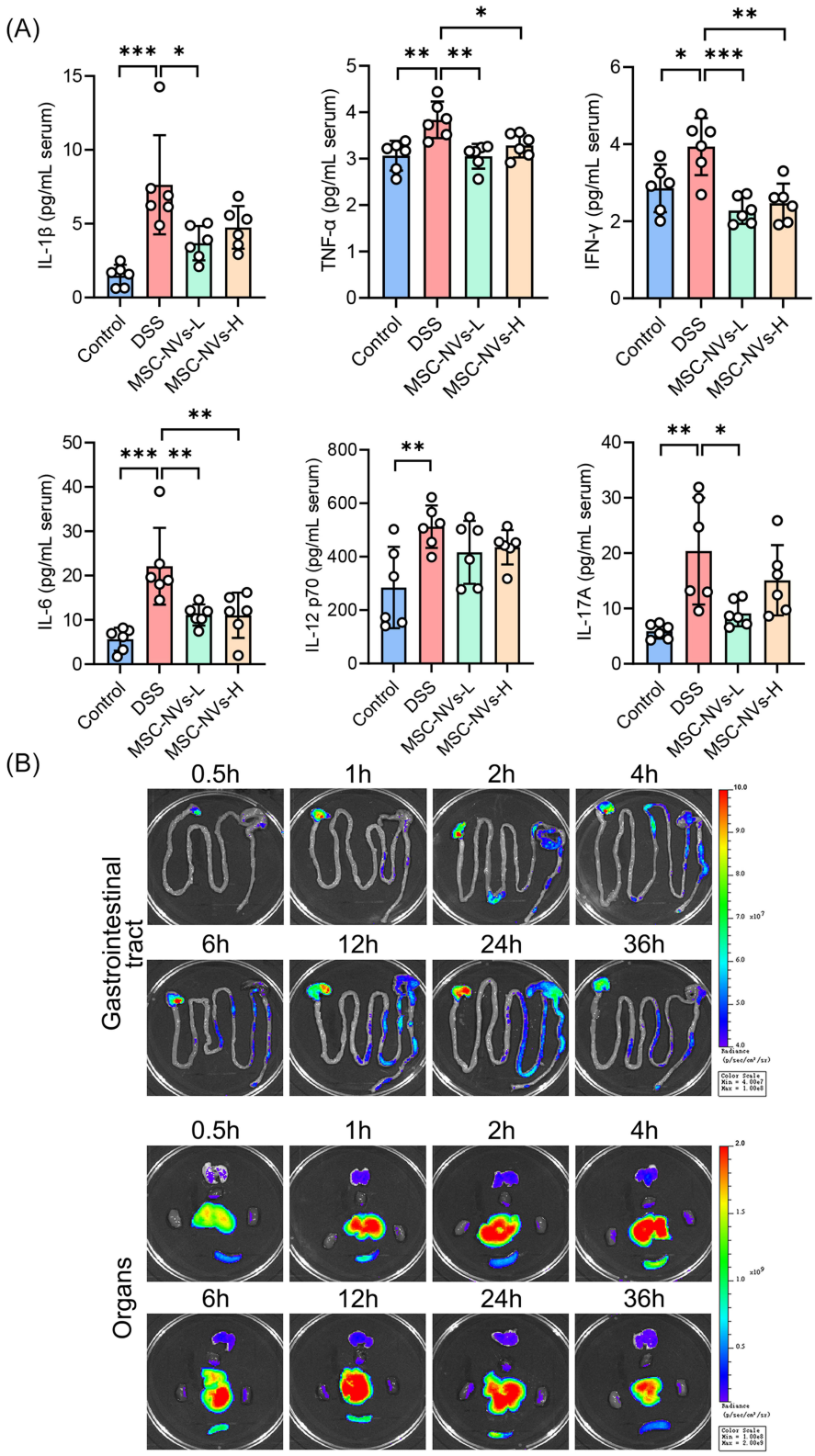

Figure 4 MSC NVs attenuated inflammation and their in vivo distribution. (**A**) Contents of the IL-1β, TNF-α, IFN-γ, IL-6, IL-12 p70, and IL-17A in the serum. (**B**) In vivo distribution of DIR-labeled MSC NVs. Fluorescent signals in the gastrointestinal tract, heart, liver, spleen, lungs, and kidneys of the mice at different time points. Means ± SD; *$p < 0.05$, **$p < 0.01$, ***$p < 0.001$.

https://doi.org/10.2147/IJN.S565416

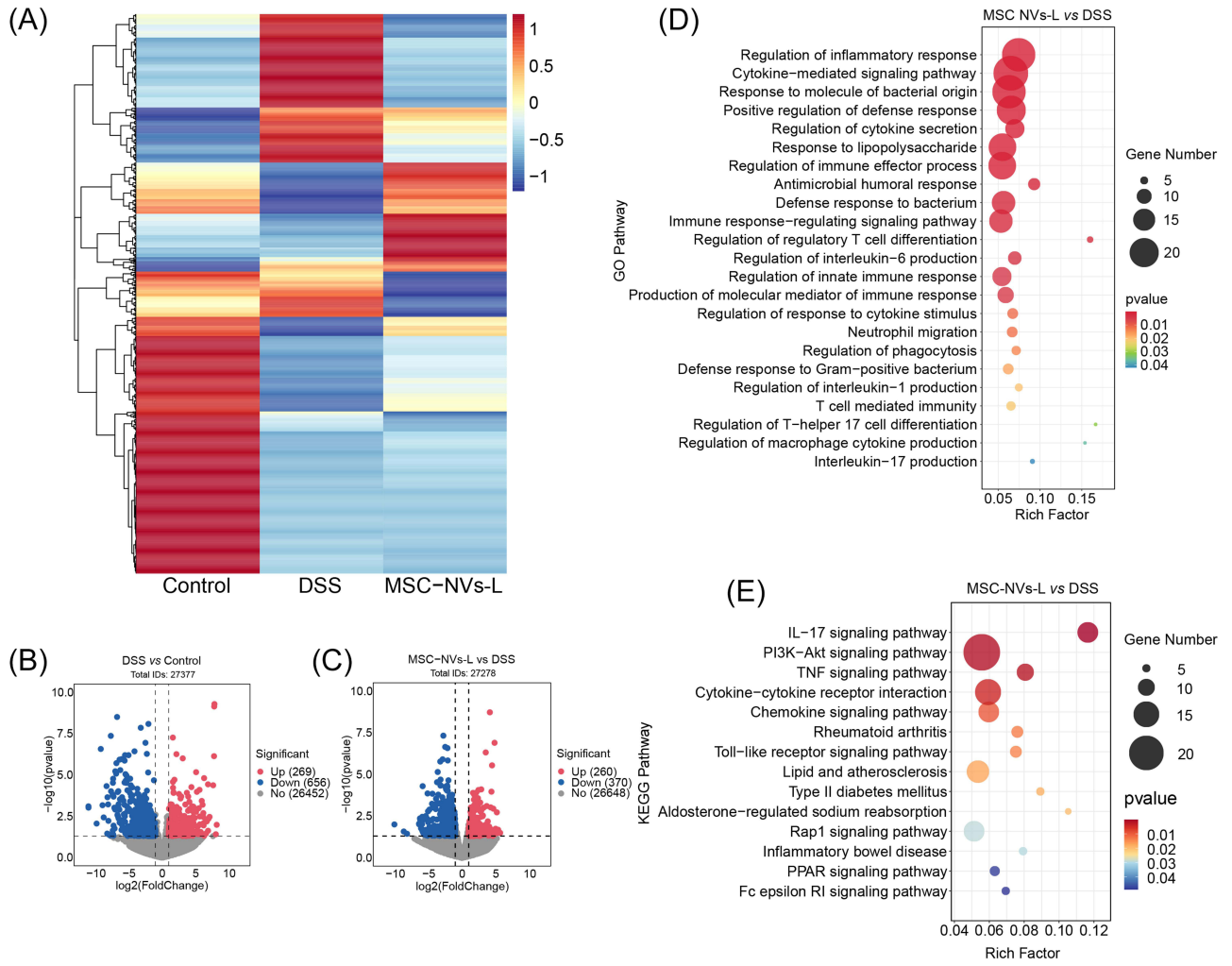

Figure 5 MSC NVs modulated the immune response in mice with colitis. (**A**) Heatmap summary of the differentially expressed genes. (**B**) Volcano plot of significantly differentially expressed genes. DSS vs Control. (**C**) Volcano plot of significantly differentially expressed genes. MSC NVs-L vs DSS. (**D**) Differential enrichment of GO pathways. MSC NVs-L vs DSS. (**E**) Differential enrichment of KEGG pathways. MSC NVs-L vs DSS.

reductions in the Shannon, Ace, Chao, and Sobs indices. Specifically, MSC-NVs significantly increased the Shannon index and Chao index (p=0.051), while other α-diversity indices remained unaffected. Regarding β-diversity, PCoA utilizing the euclidean, binary_jaccard, abund_jaccard, and bray_curtis methods all revealed distinct clustering of bacterial community compositions among the three groups, indicating significant differences between the MSC NVs-L and DSS group (Figure 6B). Venn diagram revealed that 116 OTUs were common to all three groups, while 125 OTUs were shared between the DSS and MSC-NVs-L groups (Figure 6C).

At the genus level, DSS-induced colitis resulted in a significant elevation in the relative abundance of eight bacterial genera, notably the opportunistic pathogen *Escherichia-Shigella*, concurrently with a pronounced reduction in twenty-eight genera, including the beneficial genera *Lachnoclostridium* and *Lachnospiraceae_UCG-006* (Figures 6D and 7A). Moreover, MSC NVs significantly increased the relative abundance of seven genera in the colitic microbiota, particularly promoting the proliferation of beneficial genera such as *Lachnoclostridium* and *Dubosiella* (Figure 7B). Linear discriminant analysis (LDA) of effect size (LEfSe) identified *Lachnospiraceae_NK4A136_group, Lachnospiraceae_UCG_006, Lachnospiraceae_NK4B4_group*, and *Roseburia* as the most discriminative genera in healthy controls, while colitis-associated microbiota was dominated by pathobionts including *Escherichia-Shigella, Bacteroides*, and *Helicobacter* (Figure 7C). Concurrently, MSC NVs treatment significantly enriched commensal genera including *norank_f_Muribaculaceae* (unidentified genus belonging to the family of Muribaculaceae), *Dubosiella*, and *Atopostipes* within the colitic gut microbiota.

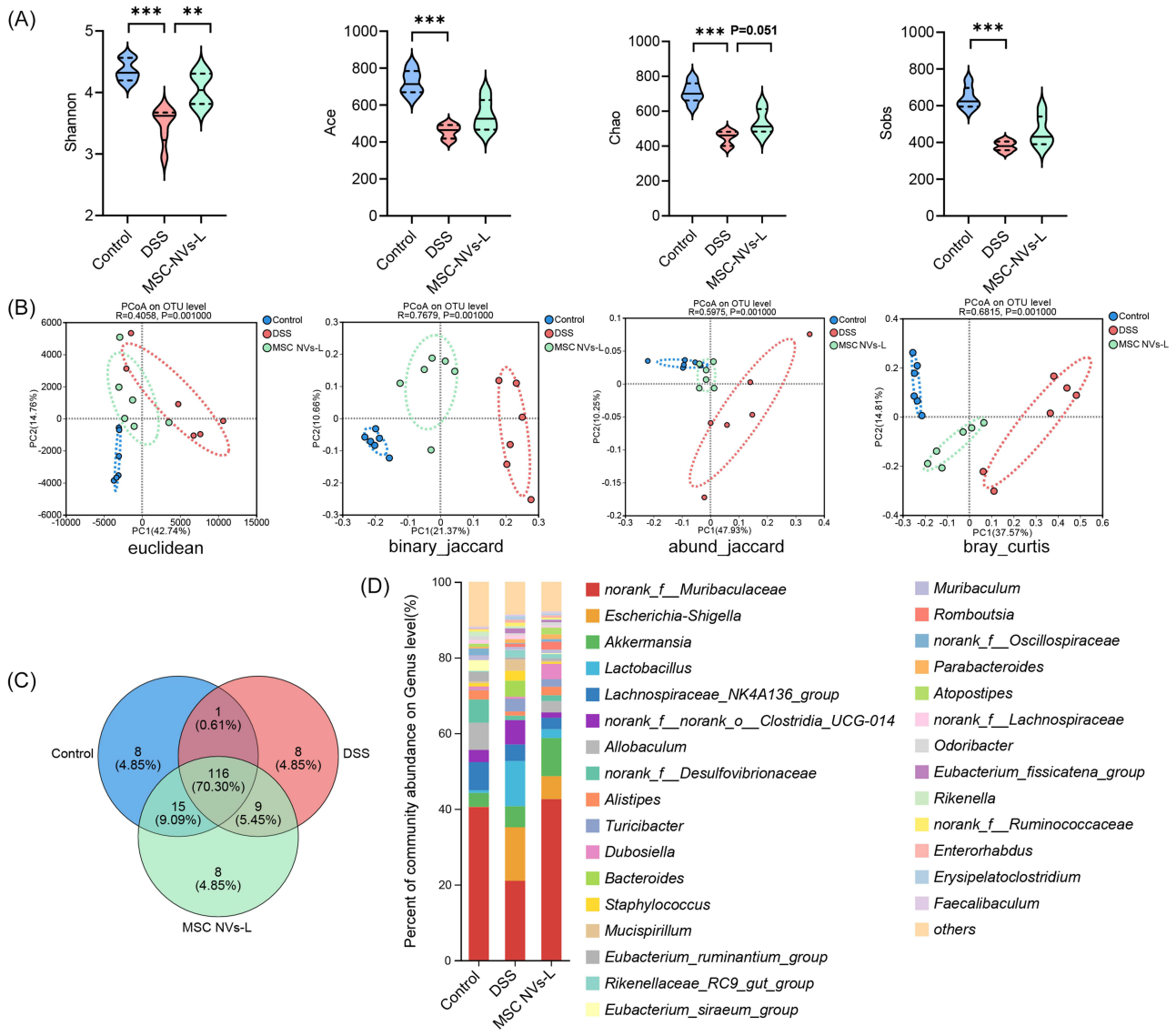

Figure 6 MSC NVs modified the microbial composition in feces. (**A**) α-diversity of microbial communities represented by Shannon, Ace, Chao, Sobs. (**B**) β-diversity of microbial communities based on the Euclidean, binary_jaccard, abund_jaccard, and bray_curtis methods. (**C**) Venn diagram. (**D**) Average relative abundance of taxa at the genus level. Means ± SD; $^{**}p < 0.01$, $^{***}p < 0.001$.

Given the well-established role of gut microbiota dysbiosis in IBD pathogenesis, the observed compositional differences in gut microbial communities between DSS-induced and MSC-NV-treated groups may underlie their distinct colitis phenotypes. Spearman correlation analysis demonstrated that *Helicobacter* abundance showed strong positive correlations with DAI scores and histological scores, along with significant associations with pro-inflammatory cytokines (TNF-α, IFN-γ, IL-6 and IL-17A). Conversely, inverse relationships were observed with body weight, colon length, and gene levels of mucin-2 and ZO-1 (Figure 7D). *Bacteroides* abundance exhibited significant positive correlations with histological score and pro-inflammatory cytokines (IL-1β and IL-6), while demonstrating negative correlations with gene levels of mucin-2, occludin and claudin-1. In contrast, *Lachnoclostridium* exhibited significant positive correlations with body weight and the gene levels of occludin and ZO-1, while exhibiting negative correlations with the DAI score and serum concentrations of TNF-α and IFN-γ. The genera *norank_f_Muribaculaceae, Dubosiella*, and *Atopostipes* exhibited significant positive correlations with body weight and the gene expression of mucin-2, occludin, claudin, and ZO-1. Additionally, *Dubosiella* and *Atopostipes* were positively associated with colon length. Conversely, these bacterial genera exhibited significant negative correlations with DAI scores, histological scores, and serum levels of IL-1β and TNF-α

https://doi.org/10.2147/IJN.S565416

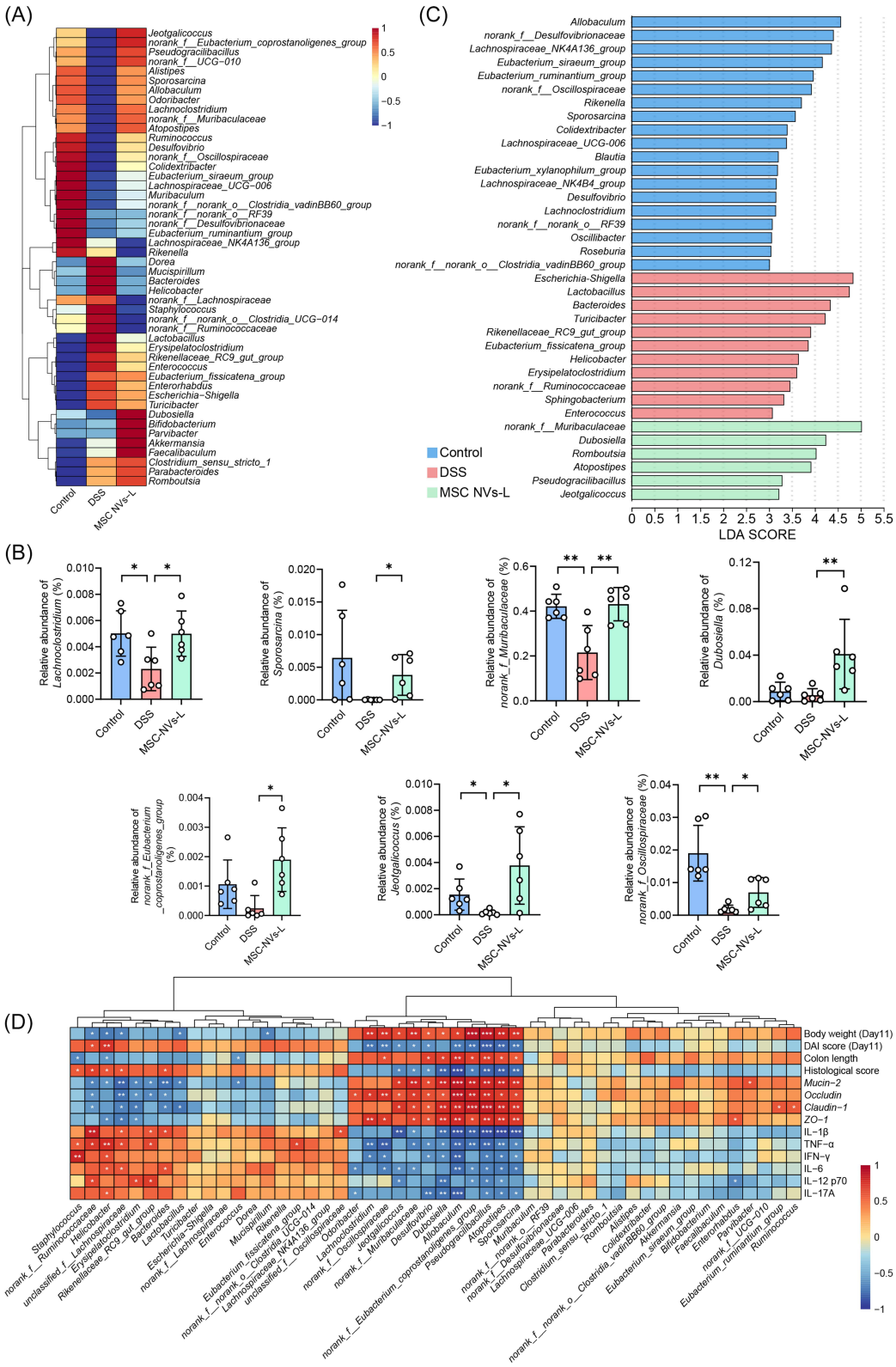

Figure 7 MSC NVs altered relative abundance of bacteria at genus level. (**A**) Heatmap of the relative abundance of the top 50 bacterial genera. (**B**) Relative abundance of bacterial genera with significant differences. (**C**) LEfSe analysis of the microbial community at genus level. (**D**) Correlation analysis between the relative abundance of the top 50 bacterial genera and phenotypes. Means ± SD; **p* < 0.05, ***p* < 0.01, ****p* < 0.001.

(*norank_f_Muribaculaceae* also exhibited a significant negative correlation with IL-6, *Dubosiella* with IFN-γ, IL-12 p70, and IL-17A, and *Atopostipes* with IFN-γ, IL-6, IL-12 p70, and IL-17A).

MSC NVs Modulated Th17/Treg Balance in Mice with Colitis

The cellular uptake of MSC NVs by Raw264.7 cells (Figure S2) demonstrated their fundamental capability to enter immune cells and suggests their potential for immunomodulation. Informed by the results of the GO and KEGG enrichment analysis results, the modulation of Th17/Treg balance in the colonic lamina propria of mice by MSC NVs was subsequently investigated. As demonstrated in Figure 8, DSS treatment significantly elevated the proportion of Th17 cells, whereas MSC NVs treatment markedly decreased Th17 cell proportion and concurrently elevated the of Treg cell proportion in colitic mice.

MSC NVs Mitigated Colitis by Modulating Th17/Treg Balance in the Colonic Mucosa Through Targeted Suppression of PI3K/Akt/STAT3 Signaling Pathway, Wherein Hsa-miR-27b-3p Served as the Key Regulatory Molecule

MicroRNAs enriched in extracellular nanovesicles serve as key regulators of biological regulations through modulating gene expression, facilitating intercellular communication, and regulating fundamental cellular physiological functions.[23,24] Consequently, the miRNA content of MSC-NVs was systematically characterized through sequencing (Figure S3). Simultaneously, KEGG enrichment analysis revealed the PI3K-AKT signaling pathway as significantly enriched among the differentially regulated genes in colonic tissues following MSC administration in colitic mice (Figure 5E). Subsequently, functional annotation of the top 20 most abundant miRNAs in MSC NVs was performed by comprehensive target prediction analysis, using StarBase, TarBase, and TargetScan databases. The functional prediction results revealed that hsa-miR-27b-3p consistently targeted the 3'UTR of PIK3CA (encoding the PI3K p110α subunit) across all three prediction databases, establishing it as a key regulator of the PI3K/AKT pathway (Figure 9A). Furthermore, hsa-miR-27b-3p exhibited evolutionarily conserved binding sites within the PIK3CA 3'UTR across multiple mammalian species, including human, mouse, and rat (Figure S4). The dual-luciferase reporter gene assay revealed that co-transfection of HEK293T cells with hsa-miR-27b-3p mimics and a wild-type PIK3CA 3'UTR plasmid (WT PIK3CA) significantly decreased luciferase activity compared to that of the negative control mimics (NC mimics). No significant reduction was observed with the PIK3CA mutated-type 3'UTR plasmid (MT PIK3CA), confirming the specificity of hsa-miR-27b-3p binding (Figure 9B). These findings conclusively demonstrate that PIK3CA is a direct functional target of hsa-miR-27b-3p. Subsequently, transfection of hsa-miR-27b-3p mimics into HEK293T

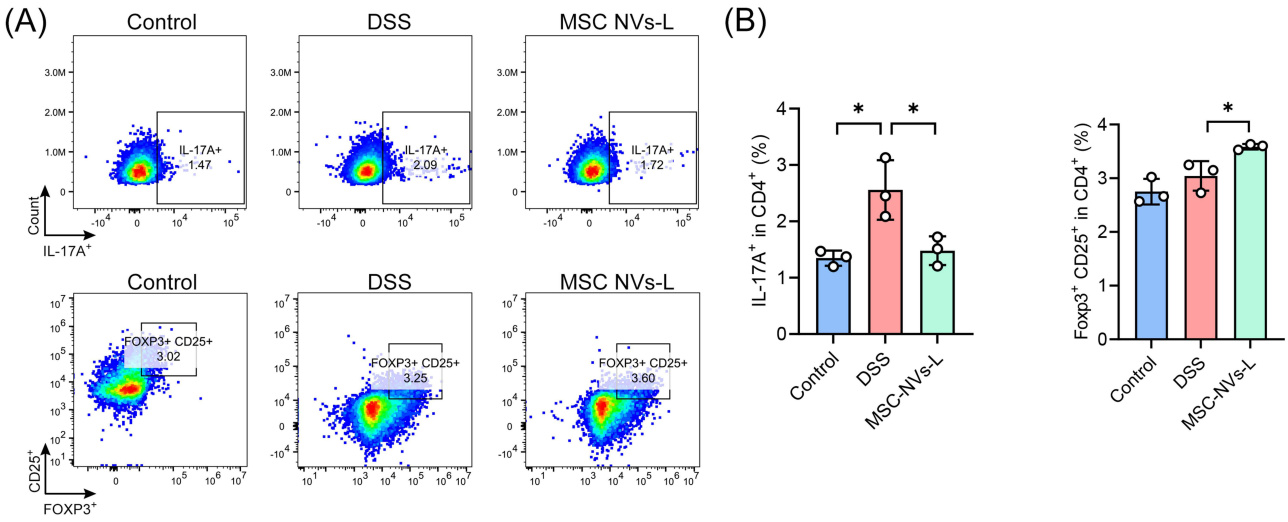

Figure 8 MSC NVs modulated Th17/Treg balance in mice with colitis. (**A**) Representative plot of Th17 ($CD45^+$ $CD3^+$ $CD4^+$ $IL\text{-}17A^+$) and Treg ($CD45^+$ $CD3^+$ $CD4^+$ $CD25^+$ $Foxp3^+$) cells in the colon lamina propria. (**B**) The percentage of Th17 and Treg cells. Means ± SD; *$p < 0.05$.

https://doi.org/10.2147/IJN.S565416

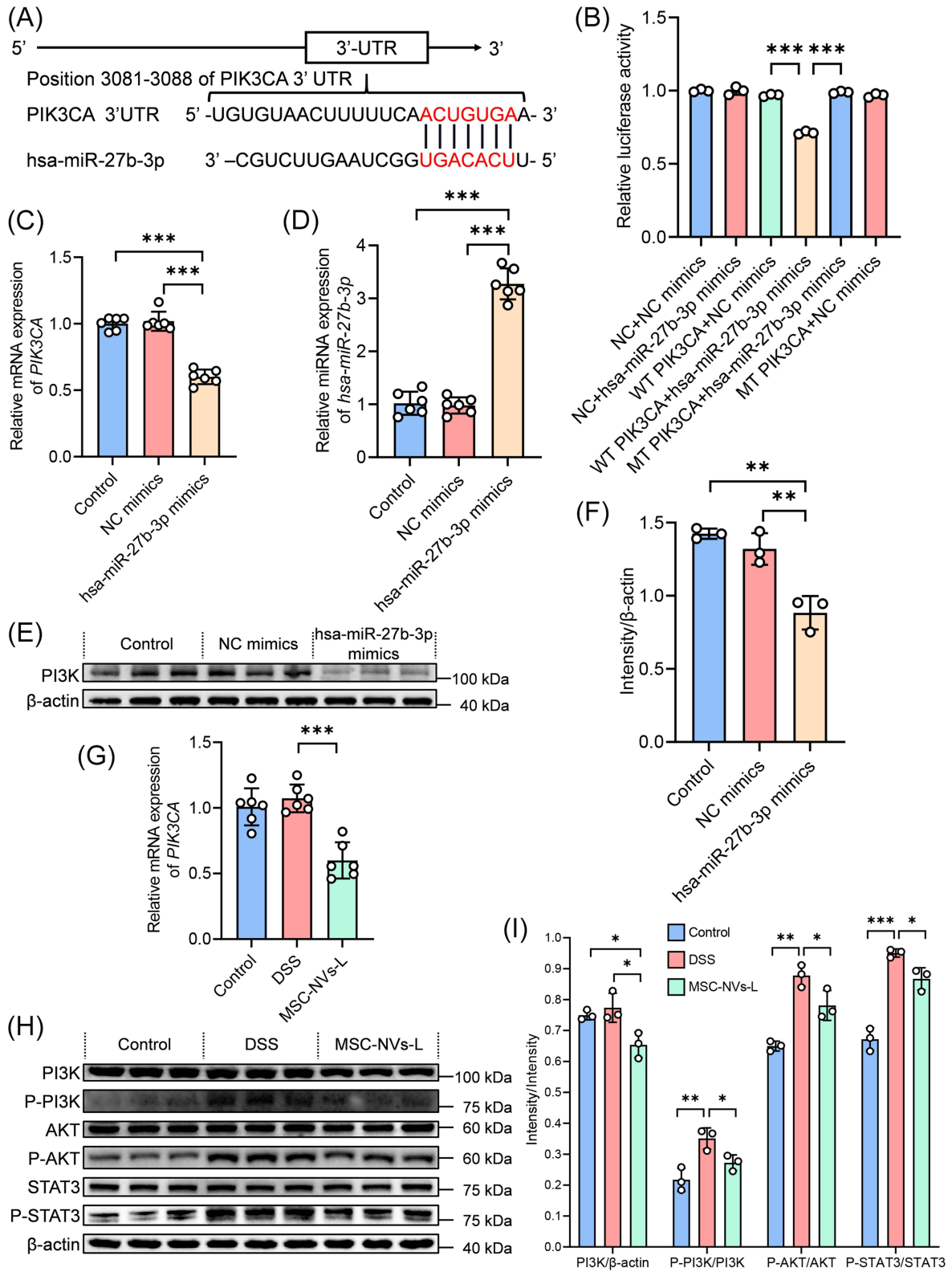

Figure 9 MSC NVs alleviated colitis through the interaction between hsa-miR-27b-3p and *PIK3CA*. (**A**) Prediction of the targeting relationship between hsa-miR-27b-3p and *PIK3CA*. (**B**) Dual-luciferase reporter gene assay. (**C**) Relative gene expression of *PIK3CA* in HEK293T cells. (**D**) Relative gene expression of *hsa-miR-27b-3p* in HEK293T cells. (**E**) Western blot of PI3K in HEK293T cells. (**F**) Quantitative analysis in Figure 9E. (**G**) Relative gene expression of *PIK3CA* in the colon. (**H**) Western blot of PI3K/AKT/STAT3 pathway in the colon of mice. (**I**) Quantitative analysis in Figure 9H. Means ± SD; *$p < 0.05$, **$p < 0.01$, ***$p < 0.001$.

cells significantly downregulated PIK3CA gene expression (Figure 9C), upregulated hsa-miR-27b-3p mimics expression (Figure 9D), and decreased PI3K protein expression (Figure 9E and F), whereas transfection of NC mimics induced no significant changes. Additionally, in colitic mice, MSC NVs treatment significantly downregulated PIK3CA expression in colonic tissue (Figure 9G), decreased PI3K protein expression, and inhibited phosphorylation of both PI3K and its downstream effectors AKT and STAT3 (Figure 9H and I).

MSC NVs Exhibit a Favorable Biosafety Profile

Favorable biosafety represents a prerequisite for clinical application of ENVs. As illustrated in Figure 10A, in vivo safety assessment demonstrated that intravenous injection of MSC NVs (MSC NVs-L: 2×10^9 particles/mouse; MSC NVs-H: 2×10^{10} particles/mouse) did not cause significant alterations in body weight (Figure 10B) and colon length (Figure 10C). Furthermore, concentrations of liver function indicators (ALT and AST) and kidney function markers (CREA and BUN) in serum remained unchanged. (Figure 10D). Moreover, histological examination revealed no apparent tissue damage or morphological abnormalities in heart, liver, spleen, lungs, kidneys and colon sections between MSC NVs-treated groups and controls (Figure 10E). The above results demonstrate that MSC NVs exhibit excellent biosafety profiles, supporting their strong potential for clinical translation.

Discussion

The current investigation demonstrated that MSC NVs, prepared using a continuous filtration–extrusion method, exert multi-faceted therapeutic effects by preserving intestinal barrier integrity, targeting inflammatory lesions, modulating immune responses, and alleviating colitis-associated intestinal microbiota dysbiosis, collectively leading to significant improvement in colitis. Mechanistically, MSC NVs ameliorated colitis via modulating colonic Th17/Treg balance through delivery of hsa-miR-27b-3p, which functionally suppresses the PI3K/AKT/STAT3 signaling pathway. Collectively, these findings demonstrate that MSC NVs as a novel class of immunomodulatory therapeutics that effectively ameliorate colitis, offering promising prospects for advancing nanomedicine and improving therapeutic outcomes in IBD treatment.

A well-formed intestinal barrier is essential for maintaining intestinal homeostasis.[25] Conversely, disturbances in critical intestinal barrier components, particularly tight junction dysregulation or goblet cell depletion, directly impair intestinal function.[26] Aberrant expression and altered distribution of tight junction proteins have been mechanistically linked to colitis progression.[1] In this investigation, MSC NVs effectively alleviated colitis symptoms, attenuating morphological and structural damage, restoring goblet cell populations, and upregulating tight junction protein expression.

Restoring the aberrant inflammatory environment of colitis constitutes an efficacious therapeutic approach. In this study, intravenous MSC NVs treatment significantly attenuated colitis-associated systemic inflammation, as evidenced by marked reductions in pro-inflammatory cytokine levels. Although both high-dose (2×10^{10} particles/mouse) and low-dose (2×10^9 particles/mouse) MSC NVs significantly alleviated colitis symptoms, the therapeutic efficacy of the high-dose MSC NVs was unexpectedly inferior to the low-dose group, indicating a non-dose-dependent therapeutic response. Similar to our findings, a clinical trial evaluating umbilical cord-derived MSCs for osteoarthritis treatment reported adverse effects (including pain or synovitis) with high-dose (8×10^7 cells), while mid- (2×10^7 cells) and low-dose (2×10^6 cells) administrations maintained therapeutic efficacy without causing any adverse reactions.[27] Matas et al observed that high-dose MSC injections might induce inflammation, which could also explain the inferior anti-colitis efficacy observed in the current study following intravenous administration of high-dose MSC NVs compared to the low-dose group. These findings indicate that further dosage optimization is required prior to clinical application of MSC NVs for colitis treatment to achieve optimal therapeutic outcomes.

Whether intravenously administered MSC NVs could specifically target and accumulate in inflamed lesions remains a critical determinant for therapeutic efficacy. In the current study, MSC NVs were observed to progressively accumulate in inflamed colonic lesions within 24 hours post-injection, thereby mediating targeted anti-inflammatory and therapeutic effects against colitis. Inflammation of the colonic mucosa leads to depletion of the mucus layer, while simultaneously causing substantial accumulation of positively charged proteins, including transferrin and antimicrobial peptides, at the site of inflammation.[28] These alterations provide molecular targets and attachment sites for negatively charged MSC NVs, thereby improving therapeutic efficacy against colonic inflammation. Furthermore, the inflammation-targeting

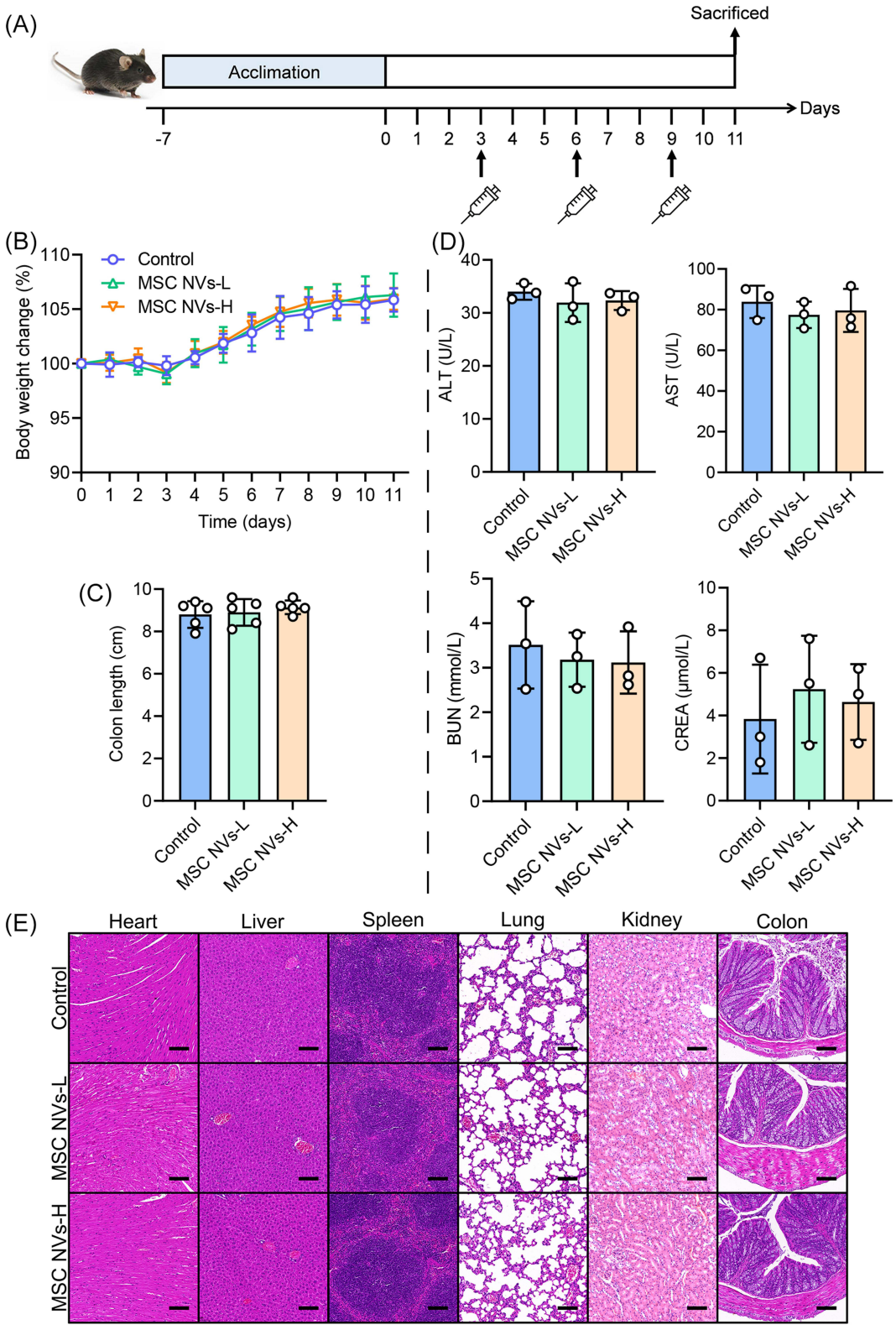

Figure 10 In vivo biosafety evaluation of MSC NVs. (**A**) Schematic illustration of biosafety assay. (**B**) Body weight change. (**C**) The length of the colon. (**D**) Serological indices of liver function (ALT and AST) and kidney function (BUN and CREA). (**E**) Representative micrographs of H&E (Scale bar, 200 μm). Means ± SD.

capability of MSC NVs may be mechanistically linked to the intrinsic tissue-homing property of parental MSCs, consequently promoting tissue repair processes.[14]

Intestinal inflammation triggers significant changes in both the gut microenvironment and microbial composition.[29] The current investigation revealed that MSC NVs significantly elevated both Shannon and Chao indices of microbiota α-diversity, reflecting improved community richness and evenness, which suggests restoration of a healthier intestinal ecosystem. β-diversity analysis revealed significant alterations in microbial community composition and structure across all groups. At the genus level, compared to the DSS group, MSC NVs treatment effectively increased the relative abundance of beneficial short-chain fatty acid-producing bacteria *Lachnoclostridium* and *Dubosiella*, indicating improved intestinal health.[30,31] Similarly, LEfSe analysis revealed distinct gut microbial compositions among the three groups. The DSS group showed enriched abundance of inflammation-associated genera: *Escherichia-Shigella* (a pro-inflammatory genus whose elevated abundance characterizes gut dysbiosis[32]), *Bacteroides* (commensal bacteria with demonstrated involvement in IBD pathogenesis[33]), and *Helicobacter* (a well-characterized contributor to IBD development[34]). Concurrently, the abundance of *norank_f_Muribaculaceae, Dubosiella*, and *Atopostipes* was enriched in the colitis mice following treatment with MSC NVs. The enrichment of *norank_f_Muribaculaceae* correlates with improved clinical recovery in UC patients.[35] *Atopostipes*, a genus of Lactobacillales order, metabolizes valine and tryptophan into branched-chain fatty acids and indole derivatives, supporting gut microbiota homeostasis.[36] Correlation analysis demonstrated that *Bacteroides* and *Helicobacter* abundance positively correlated with pro-inflammatory cytokines, whereas showing negative correlations with intestinal barrier-related proteins expression. In contrast, *Lachnoclostridium, norank_f_Muribaculaceae, Dubosiella*, and *Atopostipes* exhibited inverse correlation patterns, showing positive associations with intestinal barrier proteins and negative correlations with pro-inflammatory cytokines. Previous study has shown that ENVs-derived miRNAs can be taken up by gut bacteria and alter their composition,[37] it is postulated that MSC NVs may modulate the gut microbiota through a similar mechanism. Nevertheless, how miRNAs from intravenously administered MSC NVs interact with the gut microbiota warrants further investigation. In summary, MSC NVs effectively mitigated colitis-induced microbiota dysbiosis and promoted the restoration of a beneficial microbial profile associated with intestinal health.

The Th17/Treg balance is critical for preserving mucosal integrity and mitigating inflammation.[38] Under physiological conditions, Th17 cells secrete pro-inflammatory cytokines to support host immune defense, while Tregs are involved in the maintenance of immunological homeostasis. However, excessive or chronic of Th17 cell activation can potentiate inflammatory responses and contribute to the development of UC.[39] In the current study, MSC NVs administration significantly decreased colonic Th17 cell proportions while increasing Treg frequencies in colitic mice, indicating effective redirection of immune responses toward homeostasis and inflammation resolution. Moreover, KEGG enrichment analysis of colonic RNA sequencing data demonstrated significant enrichment of differentially expressed genes in the PI3K/AKT signaling pathway following MSC NV treatment, a pivotal regulator of Th17/Treg differentiation and function.[40–42] PI3K serves as a central regulatory enzyme within the AKT signaling pathway, governing the production of pro-inflammatory cytokines and actively driving IBD progression.[43] PI3K/AKT activation subsequently phosphorylates and activates STAT3, the master transcriptional regulator driving naïve $CD4^+$ T cell differentiation into Th17 cells.[44] Therefore, delineating the precise molecular mechanisms through which MSC NVs specifically regulate the PI3K/AKT/STAT3 signaling pathway is essential for understanding their therapeutic capacity to modulate Th17/Treg balance and alleviate colitis pathology.

MSC-derived ENVs contain a diverse repertoire of miRNAs that serve as key mediators of their immunoregulatory capacity.[45] For example, hypoxia-preconditioned MSC-derived ENVs are enriched with miR-216a-5p, which directly suppresses TLR4 expression and inhibits the TLR4/NF-κB signaling pathway, driving microglial polarization from pro-inflammatory M1 to anti-inflammatory M2 phenotypes.[46] In the current study, hsa-miR-27b-3p, a miRNA capable of targeting and regulating PIK3CA gene expression, was predicted and identified among the top 20 most abundant miRNAs in MSC NVs. The hsa-miR-27b-3p binding site within the PIK3CA 3′-UTR was validated through dual-luciferase reporter gene assays, with subsequent demonstration of PI3K protein (encoded by PIK3CA) downregulation both in vivo and in vitro. Concurrently, following intravenous injection of MSC NVs containing hsa-miR-27b-3p significantly inhibited phosphorylation of both PI3K/AKT signaling components and their downstream transcriptional regulator STAT3 in colonic tissues of colitic mice. Phosphorylation-mediated activation of the PI3K/AKT/STAT3

signaling pathway typically promotes Th17 cell differentiation, driving pro-inflammatory responses that ultimately lead to tissue damage. Conversely, intravenous injection of MSC NVs elevates Tregs proportions, consequently mitigating inflammatory responses and maintaining immune homeostasis.[47–49] In general, hsa-miR-27b-3p, an enriched miRNA in MSC NVs, mediates therapeutic effects by directly targeting the PI3K/AKT/STAT3 signaling pathway, thereby restoring colonic Th17/Treg balance. However, further investigations are necessary to precisely elucidate the mechanisms through which MSC NVs augment Treg proportions in colitis. Furthermore, studies utilizing PI3K/AKT/STAT3 pathway activators, hsa-miR-27b-3p mimics, or inhibition of endogenous hsa-miR-27b-3p are warranted to confirm that the therapeutic efficacy of MSC NVs in colitis is mediated through the restoration of Th17/Treg balance via this pathway.

Conclusions

Taken together, MSC NVs exhibited significant therapeutic efficacy in DSS-induced colitis by modulating Th17/Treg balance in the colonic lamina propria. Importantly, this study identifies hsa-miR-27b-3p as the pivotal MSC NVs-derived regulator of Th17/Treg balance, functioning through direct PIK3CA targeting and consequent suppression of PI3K/AKT/STAT3 signaling pathway activation. Overall, MSC NVs generated via continuous filtration–extrusion demonstrate considerable therapeutic potential for IBD, offering a safe, feasible, and effective treatment strategy that contributes to nanomedicine advancement.

Abbreviations

3′-UTR, 3′-untranslated region; AB-PAS, alcian blue-periodic acid-Schiff; AKT, PI3K-protein kinase B; ALT, alanine aminotransferase; AST, aspartate aminotransferase; CD, Crohn's disease; CREA, creatinine; DAI, disease activity index; DSS, dextran sulfate sodium; ENVs, extracellular nanovesicles; FBS, fetal bovine serum; GO, gene ontology; H&E, hematoxylin and eosin; IBD, inflammatory bowel disease; KEGG, kyoto encyclopedia of genes and genomes; LDA, linear discriminant analysis; LEfSe, linear discriminant analysis of effect size; miRNAs, microRNAs; MSC, mesenchymal stem cell; MSC NVs, mesenchymal stem cell-derived extracellular nanovesicles; MT, mutated-type; NC, normal control; OTUs, operational taxonomic units; PCoA, principal-coordinate analysis; PI3K, phosphatidylinositol 3-kinase; SD, standard deviation; Sobs, observed species; STAT3, signal transducer and activator of transcription 3; Th17, T help 17; Treg, regulatory T; UC, ulcerative colitis; UREA, urea; WT, wild-type.

Data Sharing Statement

All data generated or analyzed during this study are available from the corresponding author, Xiaozhou Mou and Xiaoyi Chen, upon reasonable request.

Funding

This work was supported by Science and Technology Department of the State Administration of Traditional Chinese Medicine of China - Zhejiang Province Joint Construction Project (grant no. GZY-ZJ-KJ-24098 to KTJ).

Disclosure

The authors report no conflicts of interest in this work.

References

1. Fan LN, Qi YD, Qu SW, et al. *B. adolescentis* ameliorates chronic colitis by regulating Treg/Th2 response and gut microbiota remodeling. *Gut Microbes*. 2021;13(1):1826746. doi:10.1080/19490976.2020.1826746
2. Xiao P, Zhang HL, Zhang Y, et al. Phosphatase Shp2 exacerbates intestinal inflammation by disrupting macrophage responsiveness to interleukin-10. *J Exp Med*. 2019;216(2):337–349. doi:10.1084/jem.20181198
3. Eberhardson M, Myrelid P, Söderling JK, et al. Tumour necrosis factor inhibitors in Crohn's disease and the effect on surgery rates. *Colorectal Dis*. 2022;24(4):470–483. doi:10.1111/codi.16021
4. Villablanca EJ, Selin K, Hedin CRH. Mechanisms of mucosal healing: treating inflammatory bowel disease without immunosuppression? *Nat Rev Gastroenterol Hepatol*. 2022;19(8):493–507. doi:10.1038/s41575-022-00604-y

5. Liu AR, Wang X, Liang XA, et al. Human umbilical cord mesenchymal stem cells regulate immunoglobulin a secretion and remodel the diversification of intestinal microbiota to improve colitis. *Front Cell Infect Mi*. 2022;12. doi:10.3389/fcimb.2022.960208
6. Lightner AL, Faubion WA. Mesenchymal stem cell injections for the treatment of perianal crohn's disease: what we have accomplished and what we still need to do. *J Crohn's Colitis*. 2017;11(10):1267–1276. doi:10.1093/ecco-jcc/jjx046
7. Weng ZJ, Zhang BW, Wu CZ, et al. Therapeutic roles of mesenchymal stem cell-derived extracellular vesicles in cancer. *J Hematol Oncol*. 2021;14 (1). doi:10.1186/s13045-021-01141-y
8. Han HS, Lee H, You D, et al. Human adipose stem cell-derived extracellular nanovesicles for treatment of chronic liver fibrosis. *J Control Release*. 2020;320:328–336. doi:10.1016/j.jconrel.2020.01.042
9. Zhou XH, Li T, Chen YF, et al. Mesenchymal stem cell-derived extracellular vesicles promote the proliferation and migration of breast cancer cells through the activation of the ERK pathway. *Int J Oncol*. 2019;54(5):1843–1852. doi:10.3892/ijo.2019.4747
10. Ocansey DKW, Zhang Z, Xu X, et al. Mesenchymal stem cell-derived exosome mitigates colitis via the modulation of the gut metagenomics–metabolomics–farnesoid X receptor axis. *Biomater Sci*. 2022;10(17):4822–4836. doi:10.1039/D2BM00559J
11. Wen L, Wang Y-D, Shen D-F, et al. Exosomes derived from bone marrow mesenchymal stem cells inhibit neuroinflammation after traumatic brain injury. *Neural Regeneration Res*. 2022;17(12):2717–2724. doi:10.4103/1673-5374.339489
12. Park K-S, Svennerholm K, Shelke GV, et al. Mesenchymal stromal cell-derived nanovesicles ameliorate bacterial outer membrane vesicle-induced sepsis via IL-10. *Stem Cell Res Ther*. 2019;10(1):231. doi:10.1186/s13287-019-1352-4
13. Rani S, Ritter T. The Exosome-A naturally secreted nanoparticle and its application to wound healing. *Adv Mater*. 2016;28(27):5542–5552. doi:10.1002/adma.201504009
14. Liu H, Liang Z, Wang F, et al. Exosomes from mesenchymal stromal cells reduce murine colonic inflammation via a macrophage-dependent mechanism. *JCI Insight*. 2019;4(24). doi:10.1172/jci.insight.131273
15. Ma YY, Zhao X, Chen JY, et al. Umbilical cord mesenchymal-stem-cell-derived nanovesicles as a novel strategy to promote wound healing in diabetes. *Nano Select*. 2023;4(2):170–180. doi:10.1002/nano.202200211
16. Shao T, Hsu R, Rafizadeh DL, et al. The gut ecosystem and immune tolerance. *J Autoimmun*. 2023;141:103114. doi:10.1016/j.jaut.2023.103114
17. Geuking MB, Cahenzli J, Lawson MA, et al. Intestinal bacterial colonization induces mutualistic regulatory T cell responses. *Immunity*. 2011;34 (5):794–806. doi:10.1016/j.immuni.2011.03.021
18. Liu Y-J, Tang B, Wang F-C, et al. Parthenolide ameliorates colon inflammation through regulating Treg/Th17 balance in a gut microbiota-dependent manner. *Theranostics*. 2020;10(12):5225. doi:10.7150/thno.43716
19. Cheng C, Hu J, Li Y, et al. Qing-Chang-Hua-Shi granule ameliorates DSS-induced colitis by activating NLRP6 signaling and regulating Th17/Treg balance. *Phytomedicine*. 2022;107:154452. doi:10.1016/j.phymed.2022.154452
20. D'Ambrosio A, Cossu A, Amendola A, et al. Lamina propria $CD4^+$ LAP^+ regulatory T cells are increased in active ulcerative colitis but show increased IL-17 expression and reduced suppressor activity. *J Crohn's Colitis*. 2016;10(3):346–353. doi:10.1093/ecco-jcc/jjv216
21. Kaur H, Gupta T, Kapila S, Kapila R. Protective effects of potential probiotic lactobacillus rhamnosus (MTCC-5897) fermented whey on reinforcement of intestinal epithelial barrier function in a colitis-induced murine model. *Food Funct*. 2021;12(13):6102–6116. doi:10.1039/D0FO02641G
22. Stillie R, Stadnyk AW. Role of TNF receptors, TNFR1 and TNFR2, in dextran sodium sulfate-induced colitis. *Inflamm Bowel Dis*. 2009;15 (10):1515–1525. doi:10.1002/ibd.20951
23. Bryniarski K, Ptak W, Jayakumar A, et al. Antigen-specific, antibody-coated, exosome-like nanovesicles deliver suppressor T-cell microRNA-150 to effector T cells to inhibit contact sensitivity. *J Allergy Clin Immunol*. 2013;132(1):170–181. doi:10.1016/j.jaci.2013.04.048
24. Jang E, Kim E, Son HY, et al. Nanovesicle-mediated systemic delivery of microRNA-34a for CD44 overexpressing gastric cancer stem cell therapy. *Biomaterials*. 2016;105:12–24. doi:10.1016/j.biomaterials.2016.07.036
25. Kaur H, Moreau R. Rapamycin and chloroquine insensitivity reveal mTORC1-independent regulation of epithelial permeability in differentiated intestinal Caco-2 cells. *FASEB J*. 2020;34(S1):1. doi:10.1096/fasebj.2020.34.s1.02790
26. Salim SY, Soderholm JD. Importance of disrupted intestinal barrier in inflammatory bowel diseases. *Inflamm Bowel Dis*. 2011;17(1):362–381. doi:10.1002/ibd.21403
27. Matas J, Garcia C, Poblete D, et al. A phase I dose-escalation clinical trial to assess the safety and efficacy of umbilical cord-derived mesenchymal stromal cells in knee osteoarthritis. *Stem Cells Transl Med*. 2024;13(3):193–203. doi:10.1093/stcltm/szad088
28. Zhang S, Ermann J, Succi MD, et al. An inflammation-targeting hydrogel for local drug delivery in inflammatory bowel disease. *Sci Transl Med*. 2015;7(300):300ra128. doi:10.1126/scitranslmed.aaa5657
29. Matsuoka K, Kanai T. The gut microbiota and inflammatory bowel disease. *Semin Immunopathol*. 2015;37(1):47–55. doi:10.1007/s00281-014-0454-4
30. Vital M, Howe AC, Tiedje JM. Revealing the bacterial butyrate synthesis pathways by analyzing (meta)genomic data. *mBio*. 2014;5(2):e00889. doi:10.1128/mbio.00889-14
31. Zhang Y, Tu S, Ji X, et al. Dubosiella newyorkensis modulates immune tolerance in colitis via the L-lysine-activated AhR-IDO1-Kyn pathway. *Nat Commun*. 2024;15(1):1333. doi:10.1038/s41467-024-45636-x
32. Miles SL, Holt KE, Mostowy S. Recent advances in modelling Shigella infection. *Trends Microbiol*. 2024;32(9):917–924. doi:10.1016/j.tim.2024.02.004
33. Bloom SM, Bijanki VN, Nava GM, et al. Commensal bacteroides species induce colitis in host-genotype-specific fashion in a mouse model of inflammatory bowel disease. *Cell Host Microbe*. 2011;9(5):390–403. doi:10.1016/j.chom.2011.04.009
34. Hansen R, Thomson JM, Fox JG, El-Omar EM, Hold GL. Could helicobacter organisms cause inflammatory bowel disease? *FEMS Immunol Med Microbiol*. 2011;61(1):1–14. doi:10.1111/j.1574-695X.2010.00744.x
35. Liu Y, Zhou M, Yang M, et al. Pulsatilla chinensis saponins ameliorate inflammation and DSS-Induced ulcerative colitis in rats by regulating the composition and diversity of intestinal flora. *Front Cell Infect Microbiol*. 2021;11:728929. doi:10.3389/fcimb.2021.728929
36. Cho S, Hwang O, Park S. Effect of dietary protein levels on composition of odorous compounds and bacterial ecology in pig manure. *Asian-Australas J Anim Sci*. 2015;28(9):1362–1370. doi:10.5713/ajas.15.0078
37. Teng Y, Ren Y, Sayed M, et al. Plant-Derived exosomal MicroRNAs shape the gut microbiota. *Cell Host Microbe*. 2018;24(5):637–652. doi:10.1016/j.chom.2018.10.001

38. Kaluzna A, Olczyk P, Komosinska-Vassev K. The role of innate and adaptive immune cells in the pathogenesis and development of the inflammatory response in ulcerative colitis. *J Clin Med*. 2022;11(2). doi:10.3390/jcm11020400
39. Schnell A, Littman DR, Kuchroo VK. T(H)17 cell heterogeneity and its role in tissue inflammation. *Nat Immunol*. 2023;24(1):19–29. doi:10.1038/s41590-022-01387-9
40. Lan H, Qiu W, Wu J, Hu Z, Zhang X, Zhu L. Formononetin reverses Treg/Th17 imbalance in immune-mediated bone marrow failure mice by regulating the PI3K/Akt signaling pathway. *Chin Med*. 2024;19(1):55. doi:10.1186/s13020-024-00919-9
41. Wang S, Dong Y, Zhai L, Bai Y, Yang Y, Jia L. Decreased Treg cells induced by bisphenol A is associated with up-regulation of PI3K/Akt/mTOR signaling pathway and Foxp3 DNA methylation in spleen of adolescent mice. *Chemosphere*. 2024;357:141957. doi:10.1016/j.chemosphere.2024.141957
42. Kurebayashi Y, Nagai S, Ikejiri A, et al. PI3K-Akt-mTORC1-S6K1/2 axis controls Th17 differentiation by regulating Gfi1 expression and nuclear translocation of RORγ. *Cell Rep*. 2012;1(4):360–373. doi:10.1016/j.celrep.2012.02.007
43. Razali NN, Raja Ali RA, Muhammad Nawawi KN, Yahaya A, Mohd Rathi ND, Mokhtar NM. Roles of phosphatidylinositol-3-kinases signaling pathway in inflammation-related cancer: impact of rs10889677 variant and buparlisib in colitis-associated cancer. *World J Gastroenterol*. 2023;29(40):5543–5556. doi:10.3748/wjg.v29.i40.5543
44. Weng J, Huang X, Chen X, et al. *Blocking Stat3 to Regulate the Balance of Th17/Treg in Cgvhd Therapy*. Washington, DC: American Society of Hematology; 2015. doi:10.1182/blood.V126.23.5420.5420
45. Zhang Z, Wu W, Li M, et al. Mesenchymal stem cell–derived extracellular vesicles: a novel nanoimmunoregulatory tool in musculoskeletal diseases. *Nano Today*. 2024;57:102343. doi:10.1016/j.nantod.2024.102343
46. Liu W, Rong Y, Wang J, et al. Exosome-shuttled miR-216a-5p from hypoxic preconditioned mesenchymal stem cells repair traumatic spinal cord injury by shifting microglial M1/M2 polarization. *J Neuroinflammation*. 2020;17(1):47. doi:10.1186/s12974-020-1726-7
47. Liu J, Zong C, Yu X, et al. Alanyl-glutamine (Ala-Gln) ameliorates dextran sulfate sodium (DSS)-induced acute colitis by regulating the gut microbiota, PI3K-Akt/NF-κB/STAT3 signaling, and associated pulmonary injury. *ACS Infect Dis*. 2023;9(4):979–992. doi:10.1021/acsinfecdis.3c00014
48. Huang L, Wang M, Yan Y, et al. OX40L induces helper T cell differentiation during cell immunity of asthma through PI3K/AKT and P38 MAPK signaling pathway. *J Transl Med*. 2018;16(1):74. doi:10.1186/s12967-018-1436-4
49. Koga T, Hedrich CM, Mizui M, et al. CaMK4-dependent activation of AKT/mTOR and CREM-α underlies autoimmunity-associated Th17 imbalance. *J Clin Invest*. 2014;124(5):2234–2245. doi:10.1172/JCI73411